High-momentum nucleons in finite nuclei and y scaling

Xiangdong Ji

W. K. Kellogg Radiation Laboratory, California Institute of Technology, Pasadena, California 91125

J. Engel

Norman Bridge Laboratory of Physics, California Institute of Technology, Pasadena, California 91125

Momentum distributions in several finite nuclei are calculated in the Brueckner-Bethe-Goldstone theory. For momenta larger than 0.3 GeV/c, the distributions are dominated by two-body correlations. These affect mainly the two-nucleon s-wave channels, but also slightly modify other partial waves. By mass 12 the momentum distribution is largely saturated, and by mass 28 it is very close to that of nuclear matter. The y-scaling function suggested by West is calculated and compared to that extracted from experimental quasielastic electron scattering cross sections. The existence of a discrepancy suggests that the true scaling function is not simply related to the momentum density, even in the impulse approximation.

The high-momentum components of nuclear ground-state wave functions contain valuable information about nucleon interactions and correlations. Such information is particularly important when one tries to understand the short-range behavior of the nuclear force with a fundamental theory of the strong interaction, such as quantum chromodynamics (QCD). Several authors have discussed theoretical momentum distributions in a few isolated nuclei, but a comprehensive study of mass dependence in the densities is lacking.

Recent experiments have attempted to determine momentum distributions through inclusive hadron (pion and proton) and electron scattering.[1-4] In Ref. 5, West observed that in a suitable kinematic limit the scattering is essentially one-nucleon quasielastic knockout. The cross section should scale according to a single variable y, which is a function of the energy and momentum transfer. West's scaling function is simply related to the momentum distribution of the system; under his assumptions, the high-momentum components of the nuclear wave function can be extracted in a model-independent way from the experimental cross section. The recent electron scattering experiments suggest that the y-scaling regime has been reached,[3,4] but the scaling function is not reproduced by nuclear matter momentum-distribution calculations.[6] The question of whether this discrepancy is due to the nuclear matter assumption or some other problem needs to be addressed; a systematic many-body calculation of momentum distributions in finite nuclei is clearly called for.

A brief summary of some previous momentum-distribution calculations in finite nuclei motivates our approach. Zabolitzky and Ey used the coupled cluster or exp(S) approach in the first serious many-body attack on the problem.[7] They calculated momentum distributions up to 8 fm^{-1} in ^{4}He and ^{16}O with Reid soft core, Hamada-Johnston, and de Tourreil-Sprung supersoft core

potentials, and found that beyond 2 fm^{-1} the momentum density is dominated by correlation effects. The much simpler Brueckner-Bethe-Goldstone (BBG) method[8] was later used by Van Orden, Truex, and Banerjee to calculate the momentum distribution in ^{16}O with Reid soft core and Sprung potentials.[9] The BBG results are consistent with those of Ref. 7; agreement between these two very different approaches validates the use of either one.

Here, we choose the BBG method to calculate the momentum distribution in several finite nuclei up to mass 56. The basic idea is the following: In lowest order, the nucleons are assumed to occupy a set of single-particle orbits up to the Fermi level. The single-particle wave functions are taken from a harmonic oscillator with the length parameter adjusted to fit the nuclear mean-square charge radius. (A more sophisticated choice, involving, e.g., a density-dependent Hartree-Fock calculation, will not make much difference for our purposes.) The high-momentum components contained in such a Slater-determinant wave function are small; the work of Ref. 10 shows that no single-particle model constrained to fit the charge form factor can produce enough high-momentum particles. These can only emerge from the introduction of two-body correlations. At short distances, the relative motion is dominated by the strong nucleon-nucleon repulsion, and the wave function there deviates sharply from the mean-field solution. As is well known, this effect is explicitly treated by the second-order term in the BBG hole-line expansion.[8] Including this contribution amounts to replacing the wave function of a pair of nucleons in the Slater determinant by the multiscattered two-body wave function obtained from the Bethe-Goldstone equation for finite nuclei.[11] In terms of the single-particle states ϕ_i and the "wound" wave function $\chi_{ij}(\mathbf{r}_i, \mathbf{r}_2)$, defined as the difference between correlated and uncorrelated two-body states, the momentum distribution (normalized to 1) then takes the form

$$n(k) = \frac{1}{n}\sum_i |\phi_i(k)|^2 + \sum_{i<j}\frac{2}{n}\frac{1}{(2\pi)^3}\int \chi_{ij}^*(\mathbf{r}_1,\mathbf{r})\chi_{ij}(\mathbf{r}_1',\mathbf{r})e^{i\mathbf{k}(\mathbf{r}_1-\mathbf{r}_1')}d\mathbf{r}d\mathbf{r}_1 d\mathbf{r}_1' - \sum_{i<j}\frac{1}{n}[|\phi_i(k)|^2 + \phi_j(k)|^2]$$

$$\times \int |\chi_{ij}(\mathbf{r}_1,\mathbf{r}_2)|^2 d\mathbf{r}_1 d\mathbf{r}_2 - \sum_{i<jl\neq i,j}\frac{2}{n}\text{Re}\left[\phi_i^*(k)\phi_j(k)\int \chi_{jl}^*(\mathbf{r}_1,\mathbf{r}_2)\chi_{il}(\mathbf{r}_1,\mathbf{r}_2)d\mathbf{r}_1 d\mathbf{r}_2\right], \quad (1)$$

where the summations are over all possible pairs of single-particle orbits below the Fermi level. The first term represents the momentum distribution of the simple Slater determinant. The second term contains the high-momentum components induced by correlations and is the main focus of our calculation. The third and fourth terms represent the incoherent and coherent depletion of the Fermi sea. The momentum integral of the last two terms equals that of the second so that the particle number is conserved. To make use of the solutions of the Bethe-Goldstone equation, we must transform the integral in Eq. (1) into relative and center-of-mass coordinates; for harmonic oscillator wave functions, this is conveniently accomplished with Moshinsky brackets.[12] The angular integrations can be performed analytically and a one-dimensional integral remains.

We obtain the relative wave functions in different partial-wave channels in two steps.[13] First, we solve for the two-particle relative motion in the presence of the harmonic oscillator field and Paris two-body potential. (We choose the Paris potential because with it the deuteron momentum distribution agrees with the experimental data for momenta less than 0.8 GeV/c.[14] Next we expand the true relative wave function in terms of these solutions to take into account the Pauli principle, and solve the Bethe-Goldstone equation in this "correlated basis." We treat the Pauli operator in the Eden-Emery approximation,[8] which is equivalent to angular averaging in nuclear matter calculations and under which the center-of-mass motion separates. We retain all partial waves up to $J=3$ in the subsequent momentum density calculation.

In Fig. 1 we present the calculated momentum distributions for the ^{4}He, ^{12}C, ^{28}Si, and ^{56}Ni nuclei. To fully illustrate the mass dependence, we also show the deuteron and nuclear matter momentum distributions in the same figure. The approach to nuclear matter with increasing mass is a check on our finite-nucleus calculations. For nuclei heavier than ^{28}Si, the momentum density is already very close to that of nuclear matter; one can therefore dispense with the complicated finite-nucleus considerations when discussing the experimental data in, say, ^{56}Fe.[6]

We note that the densities at k larger than about 0.3 GeV/c run parallel to the deuteron distribution. In ^{4}He, the density at high momenta is three times as big as in the deuteron, a fact that can be explained by the contribution of six s-wave channels in the summation of Eq. (1). Although the isovector s-wave contribution is not as significant as that of the isoscalar s-wave (which is produced largely by the tensor force), both are enhanced slightly in the nuclear medium, resulting in the overall factor of 3 after normalization. The momentum densities in ^{12}C increase by another factor of 2 relative to ^{4}He mainly because of other partial-wave channels that each contribute weakly but are large in number. Going to a larger mass number does not bring in more high-momentum components and the number of channels for one particle moving relative to the rest seems to saturate.

It should be pointed out that the main features of the momentum distribution discussed above have also been observed in other many-body calculations. The enhancement of the high-momentum components in ^{4}He relative to the deuteron, for instance, is noted in Ref. 7, though higher partial waves apparently contributed almost nothing there. Since the same paper demonstrated that the effects of three-hole-line and four-hole-line graphs omitted in our calculation are small, the several different calculations of high-momentum components in the nuclear ground state appear consistent with one another.

The possibility of studying these components through quasielastic electron scattering was pointed out in Ref. 15. West[5] showed that if the struck particle is initially on shell ($E=k^2/2m$) and if the final-state interaction between the knocked out particle and the residual nucleus can be neglected, the scattering cross section is then proportional to a scaling function,

$$F_1(y) = 2\pi\int_{|yw|}^{\infty} n(k)k\,dk, \quad (2)$$

where $yw = M\omega/q - q/2$ is the West scaling variable. In finite nuclei, the on-shell assumption is not realistic. Typically, the definition of y is modified to include an average nucleon binding energy ϵ (-36 MeV for ^{56}Fe) independent of momentum. With this modification the cross section still scales as Eq. (2) except now

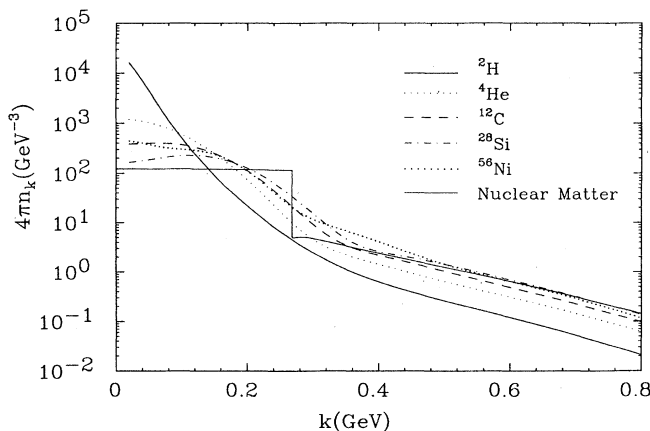$$y = -q + \sqrt{(\omega+\epsilon)^2 + 2M(\omega+\epsilon)}, \quad (3)$$

FIG. 1. The momentum distribution from Breuckner theory and the Paris potential. The nuclear matter result is taken from Ref. 6.

where we have used the relativistic energy-momentum relation.

Comparisons between the $F_1(y)$ calculated from momentum distributions in ^{4}He and ^{56}Fe, and the experimental scaling function are shown in Figs. 2 and 3. In the same figures we also show the scaling functions calculated for the deuteron and for nuclear matter. A discrepancy is apparent for y less than -0.4 GeV/c (or momenta larger than 0.4 GeV/c). The experimental $F(y)$ has a larger slope than that in the deuteron, where the agreement between theory and experiment is good[14] whereas the theoretical $F_1(y)$ curves, like the momentum distributions discussed above, are parallel to that of the deuteron. Between -0.7 GeV/c to -0.8 GeV/c, the experimental scaling function turns down to and seems to cross the deuteron function. If the scaling limit has indeed been reached experimentally, this behavior is in sharp contrast with the theoretical expectation.

If the discrepancy cannot be accounted for by finite-nucleus effects, what is its source? A careful examination of the derivation of the scaling function is necessary. The form (2) relies on the assumption that the bound nucleons all have the same separation energy ϵ. Without this assumption, a more general impulse approximation is obtained. The scattering cross section is proportional to the integral of the spectral function[3,16,17]

$$F_2(\omega,q) = 2\pi \int_{E_{max}}^{E_s} \int_{q_{min}}^{q_{max}} S(E,k)k\,dk\,dE , \qquad (4)$$

where E_{max} is essentially the energy transfer ω, E_s is the single nucleon separation energy (-10.5 MeV for ^{56}Fe), and q_{max} and q_{min} are the limits of the momentum integral,

$$q_{min} = |-q + \sqrt{(\omega+E)^2 + 2M(\omega+E)}| , \qquad (5)$$

$$q_{max} = |-q - \sqrt{(\omega+E)^2 + 2M(\omega+E)}| . \qquad (6)$$

In the large momentum transfer q limit, a scaling function

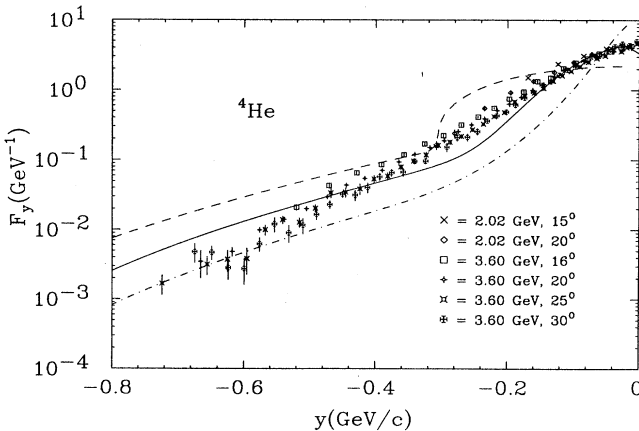FIG. 2. The scaling functions for ^{4}He calculated from the momentum distribution (solid curve). The dashed and dashed-dotted curve show the scaling function for nuclear matter and the deuteron. The experimental data is taken from Ref. 4.
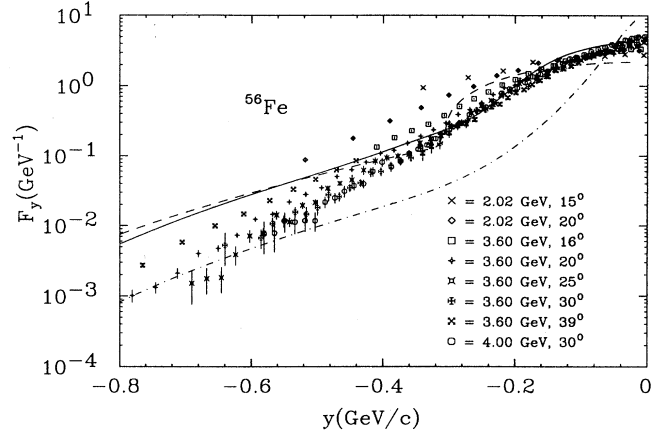
FIG. 3. Same as Fig. 2 for ^{56}Fe.

emerges,

$$F_2(y) = 2\pi \int_{-\infty}^{E_s} \int_{|y+(E-E_s)|}^{\infty} S(E,k)k\,dk\,dE , \qquad (7)$$

where

$$y = -q + \sqrt{(\omega+E_s)^2 + 2M(\omega+E_s)} . \qquad (8)$$

This definition of y differs from Eq. (3). The function $F_2(y)$ will return to the scaling function in Eq. (2) if the lower limit of the momentum integration can be replaced by $|y|$, since the sum rule for spectral function reads

$$n(k) = \int_{-\infty}^{E_s} S(E,k)dE . \qquad (9)$$

However, because the nucleons are off shell when embedded in the many-body system there are plenty of particles with energy E and momenta between $|y|$ and $|y+(E-E_s)|$ that will not contribute to the scattering because of kinematic mismatch; as a consequence $F_2(y)$ can differ from $F_1(y)$ by a large amount. The exact difference between Eq. (2) and Eq. (7) depends on the specific form of the spectral function.

These issues were recently addressed in ^{3}He, where the calculated spectral function resolves the discrepancy between $F_1(y)$ and the experimental data.[17] In heavier nuclei, Eq. (4) has never been explicitly considered, primarily because a realistic spectral function is much harder to compute. To indicate where differences between $F_1(y)$ and $F_2(y)$ may arise, we employ a simple model, the dilute hard-sphere Fermi gas. An extensive study of the single-particle properties of this system was made in Ref. 18, and in particular, the imaginary part of the single-particle self-energy was calculated analytically. The spectral function is closely related to this latter quantity and is easily computed. For k around 0.5 GeV/c, the center of the energy distribution is about 80 MeV below the Fermi surface. As k increases, the distribution moves quickly to larger separation energies; for $k = 0.8$ GeV, the center is about 280 MeV below the Fermi surface. For high-momentum particles then, the centroid energy is very low compared to ϵ, which is an average over particles of all k.

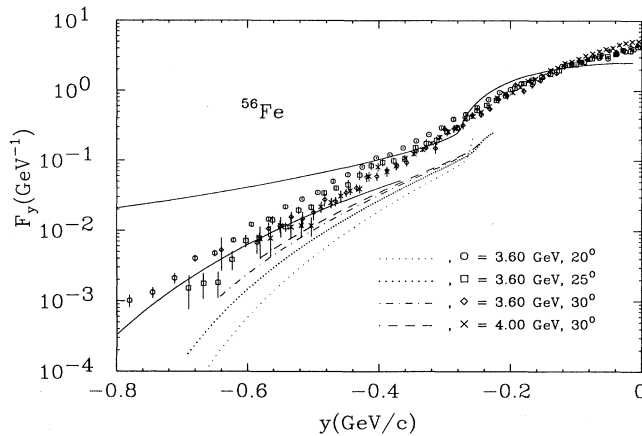The limiting scaling functions (2) and (7) for the hard sphere Fermi gas model are shown in Fig. 4. The dif-

FIG. 4. The function $F_2(\omega,q)$ calculated for the hard-sphere Fermi gas model at different kinematical conditions, and the corresponding NE3 data. The upper and lower solid curves are the limiting scaling functions defined in Eqs. (2) and (7).

ference between the two is increasingly large as $|y|$ grows. At $y = -0.8$ GeV/c, $F_2(y)$ is only about 1% of $F_1(y)$. Figure 4 also contains $F_2(\omega,q)$ calculated for the kinematic conditions applying in some of the NE3 experimental runs, along with the data.[4] The curves clearly are not yet at the theoretical scaling limit, which obtains only at very large momentum transfer (about 5 GeV in this example), and to the extent that the hard sphere calculation can be taken seriously, final-state effects add to the scaling function in the experimental region.

Of course real nuclear matter is not a hard-sphere gas. Nonetheless, it is quite plausible that many of these conclusions will apply there also. In particular, there is reason to suspect that the scaling limit has not been reached by the NE3 experiments, and that because $F_2(y)$ is so small, final-state effects still play some role. True scaling may be reached only at much larger momentum transfer, and the apparent y scaling in the data may be coincidental. Furthermore, even if the scaling regime has really been reached, the extraction of a momentum distribution relies on assumptions about the form of the spec-

tral function between $|y|$ and $|y+(E-E_s)|$. In ^{3}He, the momentum distribution turns out to be relatively insensitive to these assumptions,[17] but the many-body situation still awaits clarification.

Existing calculations of spectral functions (mostly at small momenta) employ nonrelativistic many-body theory.[19–21] However, nonrelativistic kinematics surely do not apply at the y-scaling limit. If, for example, the nonrelativistic definition of y is used,[22] the scattering cross section will not scale at all. Furthermore, the nonrelativistic scaling limit lies at time like four-momentum transfer ($\omega > q$) and cannot be reached by inelastic electron scattering. It is clear that a theoretical calculation using relativistic kinematics combined with a nonrelativistic spectral function is not satisfactory. The nonrelativistic spectral distribution peaks at about $-k^2/2m$ for large k, where the relativistic spectral distribution may peak at $-k$. These two distributions with different energy centroids could cause a large difference in the integration of Eq. (7). A relativistic spectral function seems to be necessary in a truly serious calculation. Some of the problems arising in relativistic models of y scaling have been discussed in Ref. 23.

To conclude, we have used the BBG hole-line expansion to calculate momentum distributions in finite nuclei. The mass dependence of the momentum density shows the importance of tensor correlations and nuclear saturation. Nuclear matter results obtain quickly; by mass 56, they can be used without reservation. Unfortunately, a slow approach to y scaling and the lack of a direct relation between the scaling function and momentum density may complicate attempts to extract momentum distributions from quasielastic electron scattering data. A complete understanding of the scattering requires a calculation of the nuclear spectral function, and perhaps of final-state effects as well. A relativistic approach to these quantities appears necessary for a serious comparison with the experimental data.

[1]S. Frankel, W. Frati, O. Van Dyck, R. Werbeck, and V. Highland, Phys. Rev. Lett. **36**, 642 (1976); R. Amado and R. M. Woloshyn, *ibid.* **36**, 1435 (1976).

[2]S. A. Gurvitz, TRIUMF Report No. TRI-PP-84-85 (1984).

[3]D. Day, J. S. McCarthy, I. Sick, R. G. Arnold, B. T. Chertok, S. Rock, Z. M. Szalata, F. Martin, B. A. Mecking, and G. Tamas, Phys. Rev. Lett. **43**, 1143 (1979).

[4]D. B. Day, J. S. McCarthy, Z. E. Meziani, R. Minehart, R. Sealock, S. T. Thornton, J. Jourdan, I. Sick, B. W. Filippone, R. D. McKeown, R. G. Milner, D. H. Potterveld, and Z. Szalata, Phys. Rev. Lett. **59**, 427 (1987); D. H. Potterveld, Ph.D. thesis, California Institute of Technology, 1988.

[5]G. B. West, Phys Rep. **18C**, 264 (1975).

[6]M. N. Butler and S. E. Koonin, Phys. Rev. B **205**, 123 (1988); M. N. Butler, Ph.D. thesis, California Institute of Technology, 1987.

[7]J. G. Zabolitzky and W. Ey, Phys. Lett. **76B**, 527 (1978).

[8]H. A. Bethe, Ann. Rev. Nucl. Sci. **21**, 93 (1971); J. P. Jeukenne, A. Lejeune, and C. Mahaux, Phys. Rep. **25**, 83 (1976).

[9]J. W. Van Orden, W. Truex, and M. K. Banerjee, Phys. Rev. C **21**, 2628 (1980).

[10]O. Bohigas and S. Striongari, Phys. Lett. **95B**, 9 (1980).

[11]T. T. Kuo and G. E. Brown, Nucl. Phys. **85**, 40 (1966).

[12]R. D. Lawson, *Theory of Nuclear Shell Model* (Clarendon Press, Oxford, 1980).

[13]B. R. Barret, R. G. L. Hewitt, and R. J. McCarthy, Phys. Rev. C **3**, 1137 (1971).

[14]C. Ciofi degli Atti, E. Pace, and G. Salme, Phys. Rev. C **36**, 1208 (1987).

[15]I. Sick, D. Day, and J. S. McCarthy, Phys. Rev. Lett. **45**, 871 (1980).

[16]S. Frullani and J. Mougey, Adv. Nucl. Phys. **14**, 1 (1986).

[17]C. Ciofi degli Atti, E. Pace, and G. Salme, Phys. Rev. C **39**, 259 (1989).

[18]R. Sator and C. Mahaux, Phys. Rev. C **21**, 1546 (1980).

[19]V. Bernard and C. Mahaux, Phys. Rev. C **23**, 1981 (1978).

[20]P. Grange, J. Cugnon, and A. Lejeune, Nucl. Phys. **A473**, 365 (1987).

[21]A. E. L. Dieperink, T. de Forest, I. Sick, and R. A. Brandenburg, Phys. Lett. **63B**, 261 (1976).

[22]M. N. Butler and R. D. McKeown, Phys. Lett. B **208**, 171 (1988).

[23]W. M. Alberico, A. Molinari, T. W. Donnelly, E. L. Kronenberg, and J. W. Van Orden, Phys. Rev. C **38**, 1801 (1988).